Revista Brasileira de Física, Vol. 17, nº 4, 1987

A Numerical Study of MHD Instabilities for Disruption

A. TOMIMURA
Instituto de Física, Universidade Federal Fluminense, 24210, Niterói, RJ, Brasil

Recebido em 18 de fevereiro de 1987

Abstract Numerical work has been done with a linear, one dimensional, resistive MHD code which solves a set of resistive MHD instability equations in the various relevant perturbation parameters. A number of models whose equilibrium configurations are consistent with those found in the disruptive processes in tokamaks have been considered; some of the unstable rnodes yielded by them are analysed according to their real nature (whether tearing or ideal dominated), the variation of their growth rates with q_a (the safety factor at the current channel radius) and the Magnetic Reynolds Number S (with respect to the poloidal magnetic field at the current channel radius). In particular, the conditions for the growth of the m=2, n=l mode have been studied, in a number of equilibrium configurations, taking into account the flatness of the current density profile as well as the relative value of resistivity between the current channel and the conducting wall. The tearing mode character of the unstable modes predominated in almost all cases considered, despite the high values of S and the high degree of flatness in the current density profiles used in some of the equilibrium configurations. The ideal dorninated modes could only be found in the extreme case of the step model.

1. INTRODUCTION

a) Motivation and aims

A set of resistive MHD instability equations are solved as an initial value problem in the various relevant perturbation parameters in order to investigate the growth of the most dangerous resistivemode in tokamaks viz., the m = 2, n = 1 tearing mode, regarded at present to be the main cause of the most destructive instability in tokamak experiments, known as the disruptive instability. The process of disruption is initiated by a slowly growing rnagnetic perturbation and terminates with a sudden loss of confinement; the plasma current drops to zero, for example, in JET in as little as ~20 msand sometimes slowly (1 sec) in other cases.

A code has been set up to solve the equations in a cylinder

(a straight tokamak) with a prescribed current density and resistivity profiles which can be shaped in convenient ways to reproduce, as close as possible, the equilibrium conditions found during the disruptive process. A close look has been taken to those results, which reveals (i) unstable $m=2$, n=l and $m=3$, n=2 modes with little growth rates yielded by an equilibrium configuration with a current density profile exhibiting a plateau-like distortion near the singular surface and (ii) unstable modes (tearings or kinks) which display a much faster growth rate with a flat equilibrium current density profile; the former would indicate that a tearing mode was set up creating slowly expanding magnetic islands and the latter could explain the disruptive-like nature of the instability.

b) A brief comment on major disruptive process

Major disruption has been studied by various authors in the past, each of them with a different proposal for the detailed mechanism for disruption. As seen by Turner and Wesson[1], the process of disruption begins with the onset of an $m=2$, $n=1$ and an $m=3$, $n=1$ tearing modes when the safety factor, at the plasma radius q_a, falls below a certain value (but with $q(0)$ above unity), due to an increase in the total current. Their associated islands grow around the singular surfaces defined by $q(r_s)=2$ and 3 which, in their turn, move towards the wall as the total current grows. During this motion, the current density profile presents small flattenings around the singular surfaces with the same sizes as the width of the islands. These flattenings are due to the (infinite) thermal conduction along the field lines of the islands (and nested islands) which equalizes the temperature (and therefore the conductivity) across the island. These flattenings increase the current density gradients on the inside of the singular surfaceand decrease them on the outside therefore leading to a much increased growth rate of the islands. With a further increase in the total current the value of $q(0)$ falls below unity giving rise to an $m=1$ mode with the corresponding expansion of its associated island. By the same token this again causes a flattening of the current density profile,

this time near the axis, which expands around the q=1 surface; this surface in turn moves outward as the total current keeps growing. One net effect of this process is the prevention of the extra current from accurnulating near the axis. In the meantime, the q=3 surface disappears (the m=3, n=l mode damps out) but another mode, viz., m=3, n=2 mode begins to grow at the q=1.5 surface (according to the authors it seems that this mode has little effect in the process of disruption as compared with the m=2 mode, and has been set aside froma certain pointin their analysis). While the m=1 island is still growing, the m=2 island expands and moves towards the limiter (or an outer region of cold plasma) making contact with it and cooling the outer region of the plasma colurnn. This cooling propagates inwards (through an outward heat conduction) flattening out the temperature across the island and therefore decreasing the conductivity there. Both processes therefore - growing of the m=l island and the cooling of the outer region of the plasma - have the net effect of flattening the current density profile uptothe q=1 surface and steepening it on the inside of the q=2 surfaces, enhancing the growth rate of the m=2 tearing mode even further. The m = 2 island then grows rapidly, leading to a distortion of the plasma between the two (m=2) islands with a consequent expulsion of the core of the plasma to the wall, and loss of plasma current.

Their theory is of course not complete but has the merit of giving a simple and clear picture of the disruptive process as a whole. In their theory, however, they played down the role of the m = 3, n = 2 mode for, in the region between the q=l and q=2 surfaces, this mode can be violently unstable as well as the above mentioned modes; their theory also fails to explain the disruptions that occur in some experiments where no m = 1 mode was observed (whose existence is essential to their proposed mechanism of disruption). White *et al*[2] explain the disruptive process through the growth and saturation of a large m = 2 magnetic island; although the m = 1 mode played no role in the final stage of disruption, their work left the process of the flattening of the current density profile inside the q = l surface still unexplained. They argued that it was perhaps due to the m = 1 sawtoothing process which ceased to exist 10 ms before the major disruption. Waddel *et al*[3]

proposed a mechanism for the major disruption whereby the nonlinear destabilization of tearing modes by the $m = 2$, $n = 1$ tearing mode led to the overlapping of the associated islands, with a rapid transport of heat from the center to the limiter due to the large thermal conductivity along the field lines. For their analysis they made use of a model which included mode coupling in a quasi-linear theory.

c) Outline of this work

Although none of the existing theory is complete, they all have in common the important role played by the m = 2, $n = 1$ tearing mode and the flatness of the current density profile. In this work we have no intention of proposing another mechanism for disruption; instead, we wish to understand the nature of the main unstable modes involved in the disruptive process, as well as to investigate how their growth rates evolve from one equilibrium conffguration to another. Moreover, as pointed out by D.C.Robinson[4], the growth rates of the $m=2$ modes yielded by various known equilibrium configurations are not high enough to account for the fast time scale of the disruption; thus, perhaps the final 'phase of the disruption would be caused by an ideal MHD unstable mode[5]. This possibility is also explored in the last part of this work.

To accomplish aim (i) mentioned in §(a), the entry data to run the computing code was set up to access the so-called Culham model (to be described in chapter 3) for the equilibrium configuration and in the two unstable $m=2$, $n=1$ and $m=3$, $n=2$ modes. Graphs displaying a normalized growth rate P against q_a, the safety factor at the current channel radius a, have been constructed for typical values of the input parameters. This first part of the work fixes up a standard set of results whereby all the others will be referred to. Next, to study the effect that a small plateau-like distortion on the current profile Has 'on the growth rates of the modes found before, we made use of a facility already built in the code which produces such a distortion, and whose shape and radial position can be controlled by three entry data parameters. Having chosen the position of the distortion at some radius and' using the same entry data as before, the codè was run for different

values of q_a and plots of the new growth rates against qa were compared with the corresponding ones of the standard case. Results of interest in this study are themselves part of the main results of a related work on instability control by plasma current shaping and published elsewhere[6]. For completeness sake however, this subject as well as the basic equations and assumptions used (the same as in ref.6) will be briefly summarized in the following chapters.

To accomplish aim (ii) we started from the known fact that stronger gradients on the current density profile can drive modes with increasingly large growth rates. This was achieved through two parameters of the Culham model, viz., M and N, which taylor the fiatness of the profile. By increasing this pair of numbers one can get increasingly flatter profiles (the standart Culham model uses $M=4$, $N=2$), limited only by the ability of the computer to handle large gradients. Forthis reason, the flattest profile achieved which yielded reliable numerical results was with $M=60$ and $N=32$. From then on, large rounding-off errors occurred and the code broke down. Also for this reason, we decided to consider directly the limiting case (the step model) by performing the calculation with the equilibrium profiles modelled separately, inorder to get rid of the large gradients (in this extreme case, of course, the infinite gradients are only implicit in the (finite) discontinuities of the axial current density and the field gradients). Although unrealistic the unstable *ideal* dominated modes yielded by the step model nevertheless establish limiting values for growth rates, and strongly suggest the existence of ideal modes in other flat (but not step-like) current profile which the code employed could not cope with, and which could be of some relevance to explain the major disruption.

Throughout this work we also looked at the effect caused by the value of resistivity on growth rates, by varying the magnetic Reynolds number S. In theses cases there were also upper limits set up by the code to the magnitude of S as far as the numerical precison was concerned.

2. BASIC EQUATIONS AND ASSUMPTIONS

The single fluid plasma is described in this work by the MHD

equations, viz., the continuity equation,

$$\frac{\partial \rho}{\partial t} + \nabla.(\rho \vec{v}) = 0 \ , \tag{1}$$

the equation of motion

$$\rho(\frac{\partial \vec{V}}{\partial t} + \vec{V}.\nabla\vec{V}) = \frac{\vec{J}\times\vec{B}}{c} - \nabla p \ , \tag{2}$$

Ohm's law,

$$\vec{E} + \vec{V}\times\vec{B}/c = \eta\vec{J} \ , \tag{3}$$

and by the combined Maxwell's equations and Ohm's law in the single equation,

$$\partial\vec{B}/\partial t = \nabla\times(\vec{V}\times\vec{B}) - (c^2/4\pi)\nabla\times(\eta\nabla\times\vec{B}) \ , \tag{4}$$

where ρ, $\vec{V}$, p, $\vec{J}$, $\vec{B}$, $\vec{E}$ and η are thedensity, flow velocity, scalar pressure, current density, magnetic and electric fields and resistivity respectively.

Assuming a zero flow velocity ($\vec{V}_0$=0) and denoting by subscripts (0) and (1) the equilibrium and perturbed quantities respectively one gets, for the zero order equations,

$$(\nabla\times\vec{B}_0) \times \vec{B}_0 - \nabla p_0 = 0 \ , \tag{5}$$

$$\nabla\times(\eta_0\nabla\times\vec{B}_0) = 0 \ , \tag{6}$$

and the linearized equations for the first order variables

$$\rho_0 \frac{\partial \vec{V}_1}{\partial t} = (1/4\pi)\left[(\vec{B}_0.\nabla)\vec{B}_1 - (\vec{B}_1.\nabla)\vec{B}_0 - \nabla(\vec{B}_0.\vec{B}_1)\right] - \nabla p_1 , \tag{7}$$

$$\frac{\partial \vec{B}_1}{\partial t} = \nabla\times(\vec{V}_1\times\vec{B}_0) - (c^2/4\pi)\nabla\times(\eta_0\nabla\times\vec{B}_1) \ , \tag{8}$$

where the resistivity has been assumed unperturbed and the zero order pressure has been made constant throughout the plasma radius in order to avoid rippling and interchange modes. In addition, the plasma is considered to be incompressible ($\nabla.\vec{V}_1$=0) with a constant density $\rho=\rho_0$

and in contact with the (perfectly) conducting wall,

The six equations implicit in eqs. (7) and (8) can be reduced by taking the curl of eq. (7) to eliminate the perturbed pressure p_1 and then using $\nabla.\vec{V}_1=\nabla.\vec{B}_1=0$ to eliminate V_{1z} and B_{1z} from the resulting set of equations. Now, assuming only perturbations of the form

$$f_1(r,t)\exp(im\,\Theta + ik_z z) \quad ,$$

these equations are reduced to

$$\frac{\partial B_{r1}}{\partial t} = iFV_{r1} + \frac{c^2\eta_0}{4\pi}\left[\frac{\partial}{\partial r}\left(\frac{1}{r}\frac{\partial rB_{r1}}{\partial r}\right) - hB_{r1} - \frac{2im}{r^2}B_{\Theta 1}\right] \quad , \tag{9}$$

$$\frac{\partial B_{\Theta 1}}{\partial t} = iFV_{\Theta 1} - \left[r\frac{\partial}{\partial r}\left(\frac{B_{\Theta 0}}{r}\right)\right]V_{r1} + \frac{c^2\eta_0}{4\pi}\left[\frac{\partial}{\partial r}\left(\frac{1}{r}\frac{\partial rB_{\Theta 1}}{\partial r}\right) - hB_{\Theta 1} + \frac{2im}{r^2}B_{r1}\right]$$
$$+ \frac{c^2}{4\pi}\frac{\partial \eta_0}{\partial r}\left(\frac{1}{r}\frac{\partial rB_{\Theta 1}}{\partial r} - \frac{im}{r}B_{r1}\right) \quad , \tag{10}$$

$$-4\pi\rho_0 i\frac{\partial}{\partial t}\left[\frac{\partial}{\partial r}\left(\frac{1}{r}\frac{\partial rV_{r1}}{\partial r}\right) - hV_{r1} - \frac{2im}{r^2}V_{\Theta 1}\right]$$
$$= F\left[\frac{\partial}{\partial r}\left(\frac{1}{r}\frac{\partial rB_{r}}{\partial r}\right) - hB_{r1} - \frac{2im}{r^2}B_{\Theta 1}\right]$$
$$+ \left[-\frac{m}{r^2}\frac{\partial}{\partial r}\left(r\frac{\partial B_{\Theta 0}}{r}\right) - \frac{m}{r^3}B_{\Theta 0} - k_z r\frac{\partial}{\partial r}\left(\frac{1}{r}\frac{\partial B_{z0}}{\partial r}\right)\right]B_{r1}$$
$$+ \left[-\frac{2m}{r^2}B_{\Theta 0}\right]\frac{\partial B_{r1}}{\partial r} + \left[-\frac{2h}{r}B_{\Theta 0}\right]iB_{\Theta 1} \quad , \tag{11}$$

and

$$-4\pi\rho_0\frac{\partial}{\partial t}\left[\frac{\partial}{\partial r}\left(\frac{1}{r}\frac{\partial rV_{\Theta 1}}{\partial r}\right) - hV_{\Theta 1} + \frac{2im}{r^2}V_{r1}\right]$$
$$= -iF\left[\frac{\partial}{\partial r}\left(\frac{1}{r}\frac{\partial rB_{\Theta 1}}{\partial r}\right) - hB_{\Theta 1} + \frac{2im}{r^2}B_{r1}\right]$$
$$- \left[\frac{1}{r}\frac{\partial}{\partial r}(rB_{\Theta 0})\right]\left[\frac{\partial}{\partial r}\left(\frac{1}{r}\frac{\partial rB_{r1}}{\partial r}\right) - hB_{r1}\right]$$

$$- \left[\frac{1}{r^2}\frac{\partial}{\partial r}\left(r^2\frac{\partial^2 B_{\Theta 0}}{\partial r^2}\right) + \left(\frac{2m^2-1}{r^2}\right)\frac{\partial B_{\Theta 0}}{\partial r} + \frac{B_{\Theta 0}}{r^3} + \frac{2mk_z}{r}\frac{\partial B_{z0}}{\partial r}\right] B_{r1}$$

$$- \left[2\frac{\partial}{\partial r}\left(\frac{1}{r}\frac{\partial r B_{\Theta 0}}{\partial r}\right)\right]\frac{\partial B_{r1}}{\partial r} - \left[2\left(\frac{m}{r}\frac{\partial B_{\Theta 0}}{\partial r} + k_z\frac{\partial B_{z0}}{\partial r}\right)\right] i\frac{\partial B_{\Theta 1}}{\partial r}$$

$$+ \left[-\frac{m}{r^2}\frac{\partial}{\partial r}\left(r\frac{\partial B_{\Theta 0}}{\partial r}\right) + \frac{3m}{r^3}B_{\Theta 0} - \frac{k_z}{r}\frac{\partial}{\partial r}\left(r\frac{\partial B_{z0}}{\partial r}\right)\right] iB_{\Theta 1} \quad , \qquad (12)$$

where

$$F = \frac{mB_{\Theta 0}(r)}{r} + k_z B_{z0}(r) \quad \text{and} \quad h = \frac{m^2}{r^2} + k_z^2 \ .$$

An existing code[(a)] is then employed to solve these equations with a suitable set of boundary conditions for the $m \geq 2$ modes, viz., $B_{r1} = B_{\Theta 1} = V_{r1} = V_{01} = 0$ at $r=0$, $B_{r1} = V_{r1} = 0$ at $r = R_w$ (the conducting wall),

$$B_{\Theta 1} = \frac{imR_w}{m^2 + k_z^2 R_w^2}\left.\frac{\partial B_{r1}}{\partial r}\right|_{r=R_w}$$

$$V_{\Theta 1} = \frac{imR_w}{m^2 + k_z^2 R_w^2}\left.\frac{\partial V_{r1}}{\partial r}\right|_{r=R_w}$$

provided $\vec{k}.\vec{B} \neq 0$ at the wall and the pressure $p_1 \to 0$ as $r \to R_w$.

In so far as boundary conditions are concerned we point out that no provisions have been made to include a vacuum region betweenthe plasma and the wall, although one can simulate a vacuum by raising the resistivity from the current channel radius $r=a$ to the conducting wall and yet maintaining the same boundary conditions.

Now, as one can see from eqs. (9)-(12), the coefficients of the resulting set of equations depend on the equilibrium parameters $B_{\Theta 0}(r)$, $B_{z0}(r)$ and their derivatives. These are either given as numerical data from the experiments or by modelling the equilibrium configuration from a given profile of a relevant parameter and deriving all

(a) at Culham Laboratory, named RIPPLE4A - see also refs.7-9.

others through Maxwell's equations. A number of equilibrium models have been adopted in the past by various authors[8-13] to study MHD instabilities and amongst them we chose the Culham model for its versatility in reproducing most of the profiles observed in the experiments.

For computation, both the perturbation and the equilibrium equations are written in normalized forms in terms of the normalized independent variables $x=r/a$ and time $\tau=t/\tau_R$ and the dependent variables $\psi=B_{r1}/B$, $\phi = iB_{\theta 1}/B$, $W= -ik\tau_R V_{r1}$ and $U=k\tau_R V_{\theta 1}$. Here, a is the current channel radius, $\tau_R=4\pi L^2/c^2<\rho>$ is the resistive diffusion time, L and $<\eta>$ being the characteristic length (equal to a in our case) and resistivity respectively, $k=(m^2/R_s^2 + k_z^2)^{1/2}$, R_s standing for the radial position of the singular surface and $B(=2B_{\theta a})$ the characteristic value of the magnetic field. The free parameters for the input data are the safety factor at the current channel position $q_a=q(1)=\tilde{B}_z(1)/\tilde{R}_0\tilde{B}_O(1)$, with $\tilde{B}_z(1)$, $\tilde{B}_O(1)$ and $\tilde{R}_0=R_0/a$ standing for the normalized z and O componènts of the magnetic field and major radius respectively, the magnetic Reynoldsnumber $S=\tau_R/\tau_H$, where $\tau_H=L(4\pi<\rho>)^{1/2}/B$ stands for the Alfvén transit time with $<\rho>$ being the characteristic density (set equal to ρ_0 in this work), the mode numbers m and n, the tokamak approximation for the wave number, $k_z=-n/R_0$, and the normalized wall radius $\tilde{R}_W=R_W/a$.

Finally, chosen the equilibrium model, an initial perturbation and the input data, the code treats the system of eqs. (9) - (12) together with the boundary conditions, as an initial-boundary value problem, making use of a finite-difference scheme for the four (normalized) equations for B_{r1}, $B_{\theta 1}$, V_{r1} and $V_{\theta 1}$ by reducing them to a single vector difference equation and solving them simultaneously at each integral time step; the normalized growth rate $P=(\partial\psi(x,\tau)/\partial\tau)/\psi$, with ψ standing for any of the four normalized variables mentioned above, is also calculated at each time step ($P=\gamma\tau_R$, where y is theoriginal growthrate). For graphics, the representative profiles of the eigenmode are further normalized, each one to its maximum or minimum value.

3. THE STANDARD AND MODIFIED CULHAM MODEL

In order to accomplish aim (i) mentioned in I.§a, anequilibrium

model based on the measured temperature profile on the T3-A tokamak was constructed in which the current density has the form

$$J_{z0} = \begin{cases} J_0 \left[1-(r/a)^M\right]^N & , \quad r \leq a \\ 0 & , \quad r \geq a \end{cases} \tag{13}$$

where N and M were made equal to 2 and 4 respectively, a is the current channel radius and J_0 is a normalization factor. The set' of algebraic expressions for $J_{\Theta 0}$, $B_{\Theta 0}$ and B_{z0}, easily obtained from Maxwell's equations, constitute the Culham model for the equilibrium. The modified Culham model is obtained from the standard one described aboveby superimposing on its (smooth) poloidal magnetic field $B_{\Theta 0}$ a gaussian-like function, viz., $B_{\Theta 0}(r) + S_1 \exp\left[-S_2 (r-RR_1)^2\right]$, with the $J_{z0}(r)$ current density now adjusted by Ampère's law. The latter displays a dip on its radial profile whose height, width and radial position are controlled by $S_1(<0)$, $S_2(>0)$ and RR_1 respectively.

Now, although the variation of the growth rates of the resistive modes as a function of the safety factor q_a and the magnetic Reynolds number S, as well as the nature of the instabilities for both models, have been studied in ref.6 from another viewpoint, viz., control of the instability, we can nevertheless extract from that work the results which serve our purpose for the present one, For completeness sake therefore, we repeat such results below, beginning with the ones depicted in fig.1 where the growth rate P of the unstable modes found by the code is plotted aqainst the magnetic Reynolds number S, with all the other entry data fixed at $\tilde{R}_w$=1.4, k_z=-0.25, $\tilde{R}$ =4., $(N,M)=(2,4)$ with q_a= =2.4 for a series of running for the m=2, n=l modes and with q_a = 1.8, R_z =-0.50 for another series for the m=3, n=2 modes. As one can see from the figure, the linear behaviour (in log vs. log space) shows up above S - 3000; if we describe this range of variation by the formula $P \propto S^K$, the value of K is 0.76 for the m=2 mode and 0.756 for the m=3 mode. This is well above the sheet pinch[10] value whose growth is given by $P \propto S^{2/5}$, but only a fraction greater than the value K=0,74 predicted in the peaked model[13].

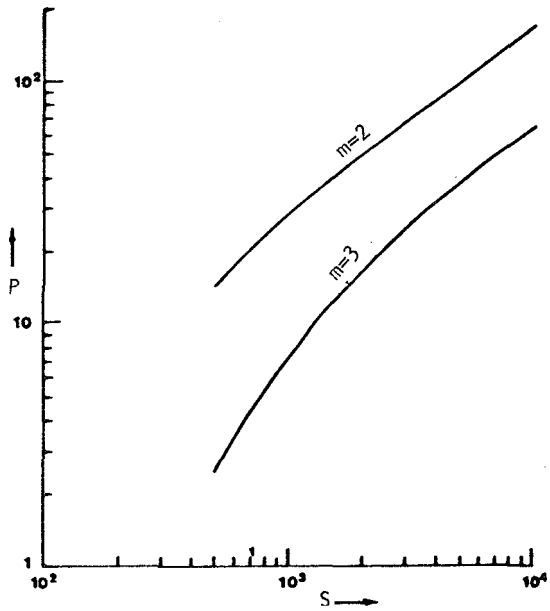

Fig.1 - Growth rate P versus S for the modes m=2, n=1 with q =2,4 and m=3, n=2 with q_a=1.8.

Figures 2 and 3 show that it is possible to inhibit or even suppress one of the modes (m=2 or m=3). For comparison the dashed curves standing for the standard Culham model (N=2, M=4) are also exhibited. The x_s curves show that the singular surfaces are, in both cases, away from the wall, showing that the boundary conditions are being satisfied. Now, although no overlapping of the stability windows occurs, it would be interesting to exploit this possibility by playing with the prescribed deformation of the current profile. This is the viewpoint adopted in ref.6. However, these curves can also be seen as the variation of the growth rates with q_a when the magnetic islands begin to grow around the q=2 and q=3/2 singular surfaces. An accurate analysis (see chapter 4 for the method) shows that all the modes found with either the standard or the modified model are tearing-like in nature. The ones depicted in fig. 4(d) represent the perturbation profiles of one run of the modified model for the m=2 mode with q_a=2.2 and whose equilibrium is

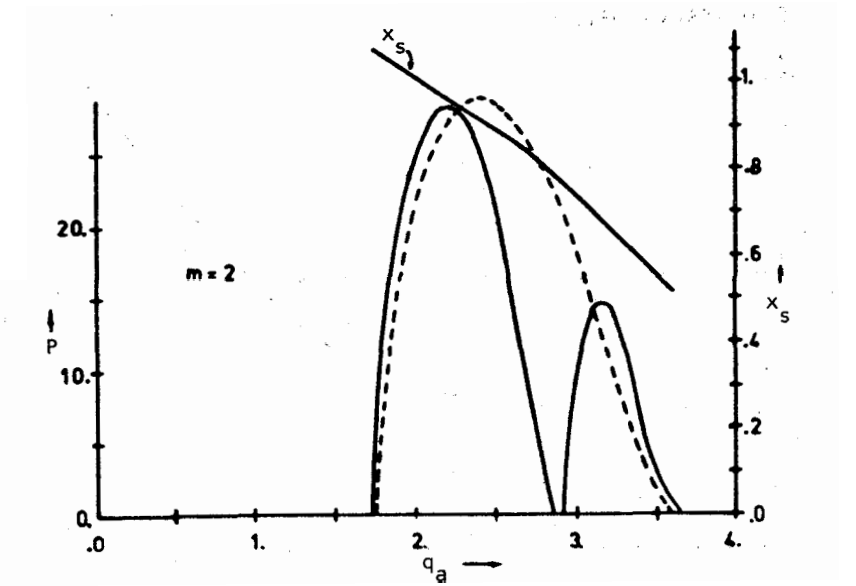

Fig.2 - The normalized growth rate P and the singular surface radius x_s as a function of q_a for the rnodified Culham mdel and the m=2, n=l mode with (Si, S_2, RR_1) = =(-0.013, 75.0, 0.7); the curve in broken lines represent the standard mdel results.

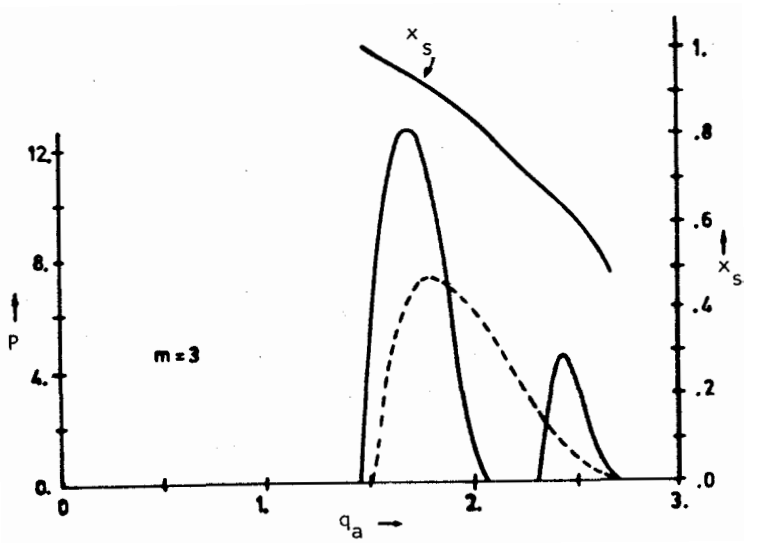

Fig.3 - As for fig.2, except m=3, n=2.

EQUILIBRIA PROFILES

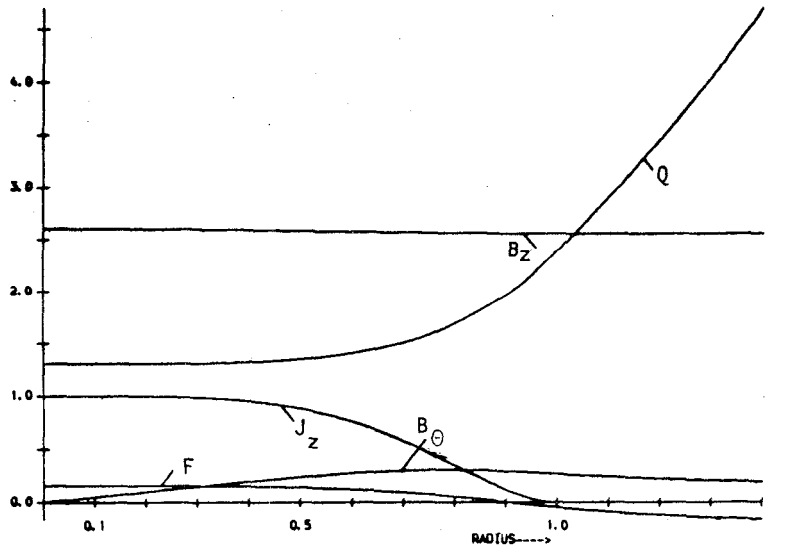

4(a)

B_{zo}=2.60718, B_{za}=2.56000, B_{ta}=0.26702, R_s=0.90728, F_o=0.15695, Q_o=1.30359

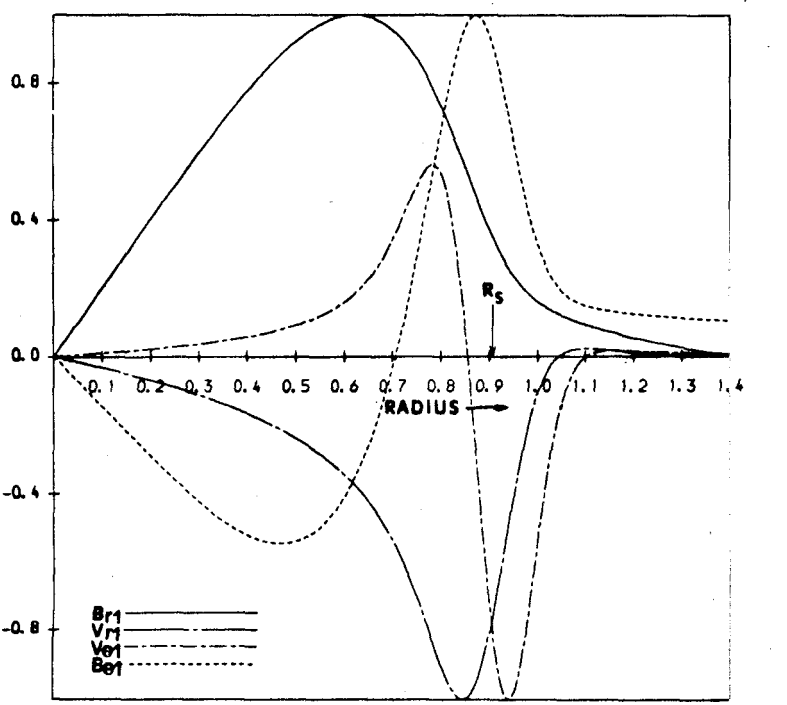

4(b)

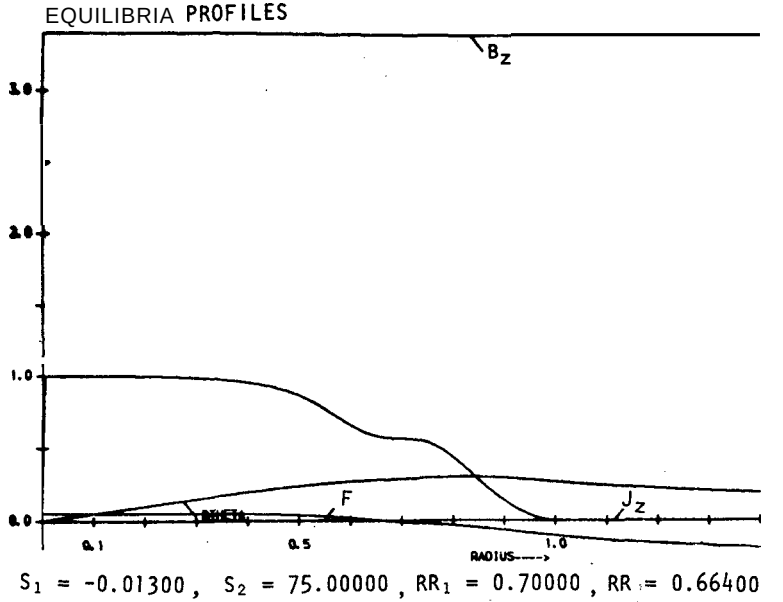

4(c)

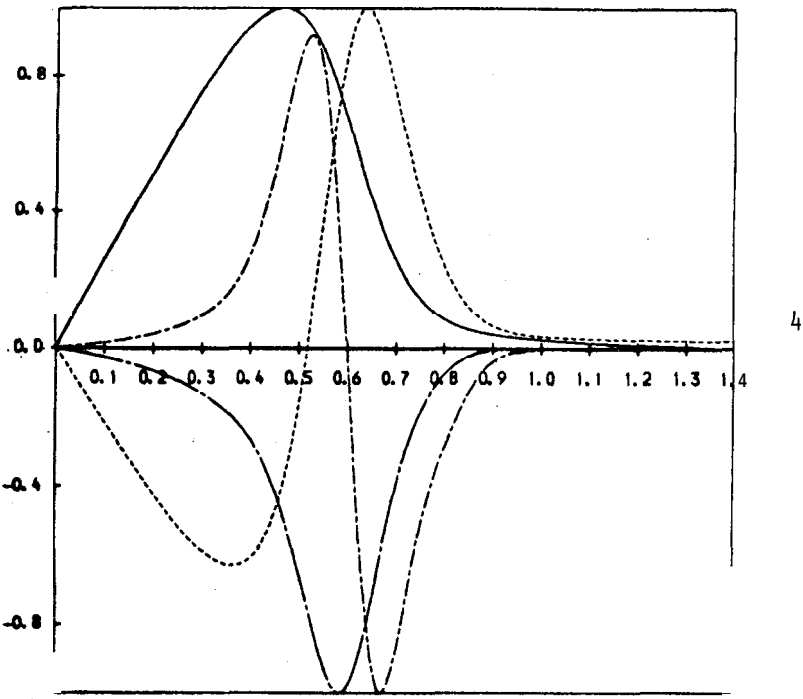

4(d)

Figs.4 - (a) Equilibria and (b) perturbed normalized orofiles for the mode m=2, n=l and S=1000 along the normalized radius,' for the standard Culham rnodel with q_a=2.4; (c) equilibria and (d) perturbed profiles for the same mode and q_a=2.2 for the modified rnodel.

shown in fig.4(c). For comparison, the same mode yielded by the standard model with q_a=2.4 is also shown in figs.4(a) and (b). Both represent the greatest growing mode for each model. These are the modes whichplay a role in the initial phase of disruption. As the islands grow, the flattening process on the current profile outwards from the axis takes place and the mode grows with a much enhanced rate. A study of the equilibrium configurations and modes which bear these characteristics will be described next.

4. THE SEARCH FOR THE FASTEST GROWING MODE

This part of the work is mainly concerned with the search of the m=2, n=l unstable modes, which could be identified with those modes which might explain the process of major disruption by virtue of their unusually large growth rates, During this search, we also looked at the nature of the modes for, as pointed out by D.C.Robinson[5], thedisruption might be caused by an ideal (kink) mode. Moreover, according to B. V. Waddel et al[3] the q profiles observed in the PLT tokamak before a disruption suggest that one should look for unstable modes yielded by an equilibrium configuration which presents a flat current profile. We start therefore with an equilibrium model which can provide us with the appropriate flat current profile and, for some fixed q_a, by lookingatthe variation of the growth rates and changes in the perturbation profiles as S is increased. More specifically, if with an increase in S, the profile of B_{r1} near the wall depresses towards the axis (eventually crossing it) and the point where V_{r1} crosses the axis moves towards the wall (or eventually maintains the same sign), then we have a typical case of a kink-dominated mode; otherwise, if the form of B_{r1} does not change significantly and the point where V_{r1} crosses the axis moves towardsthe singular surface, then we have a tearing-dominated mode. This method has been used in the past[5,6] and will also be used in this work to identify the real nature of the unstable modes found in the computation.

(a) Numerical results for a flat current profile

As noted previously, a flat current profile $J_{z0}(r)$ can be

achieved by using large values for the pair (N,M) in the Culham model. There is a limitation however, to how large these numbers can be, imposed by the cornputer. This is because these numbers appear in combinatorial forms in the calculation of the equilibrium profiles of $B_{z0}(r)$, $B_{00}(r)$ and their derivatives and one has to be careful in not exceeding the capacity of the machine in dealing with large nurnbers. In the old Culham rnodel, all the equilibrium quantities as well as their derivatives were written in terms of sums derived from the summation formulas for $J_{z0}(r)$, $B_{z0}(r)$ and $B_{\Theta 0}(r)$, and this fact was a major source of numerical errors and the eventual code breakdown, The modification introduced to minimize these problems consisted of using a Pascal triangle property to generate the combinatorial numbers to be used in the (rewritten) formulas for $\tilde{B}_{\Theta 0}$ and $\tilde{B}_{z0}$, derived from the normalized current density, $\tilde{J}_{z0}(x)=(1-x)^{M})^{N}$, $x \leq 1$, $\tilde{J}_{z0}(x)=0$, $x \geq 1$, viz.,

$$\tilde{B}_{\Theta 0}(x) = \begin{cases} \sum_{K=0}^{N} \dfrac{(-)^K C_{N,K}}{(KM+2)} x^{KM+1} , & x \leq 1 \\ \tilde{B}_{\Theta 0}(1)/x , & x \geq 1 \end{cases} \tag{14}$$

$$\tilde{B}^2_{z0}(x) = \begin{cases} \tilde{B}^2_z(1) + \sum \dfrac{(-)^{L+K} C_{N,K} C_{N,L} \left[1 - x^{(K+L)M+2}\right]}{(KM+2)\left[(K+L)M+2\right]} , & x \leq 1 \\ \tilde{B}^2_z(1) , & x \geq 1 \end{cases} \tag{15}$$

and using known expression derived from pressure balance and Ampère's law to calculate the derivatives, viz.,

$$\tilde{B}'_{\Theta 0} = \tilde{J}_{z0} - \tilde{B}_{\Theta 0}/x , \tag{16}$$

$$\tilde{B}''_{\Theta 0} = \tilde{J}'_{z0} - (\tilde{J}_{z0} - 2\tilde{B}_{\Theta 0}/x)/x , \tag{17}$$

$$\tilde{B}'''_{\Theta 0} = \tilde{J}''_{z0} - \tilde{J}'_{z0}/x + 3(\tilde{J}_{z0} - 2\tilde{B}_{\Theta 0}/x)/x^2 , \tag{18}$$

$$\tilde{B}'_{z0} = - \tilde{J}_{z0} \tilde{B}_{\theta 0}/\tilde{B}_{z0} \quad , \tag{19}$$

$$B''_{z0} = \tilde{B}_{\theta 0}\tilde{J}_{z0}\tilde{B}'_{z0}/\tilde{B}^2_{z0} - (\tilde{B}_{\theta 0}\tilde{J}'_{z0} + \tilde{J}_{z0}\tilde{B}'_{\theta 0})/\tilde{B}_{z0} \quad , \tag{20}$$

$$\tilde{B}'''_{z0} = \tilde{B}_{\theta 0}\tilde{J}_{z0}\tilde{B}''_{z0}/\tilde{B}^2_{z0} - \tilde{B}_{\theta 0}\tilde{J}''_{z0}/\tilde{B}_{z0} - \tilde{J}_{z0}\tilde{B}''_{\theta 0}/\tilde{B}_{z0} - 2\tilde{B}'_{\theta 0}\tilde{J}'_{z0}/\tilde{B}_{z0} -$$

$$- 2\tilde{B}_{\theta 0}\tilde{J}_{z0}\tilde{B}'^2_{z0}/\tilde{B}^3_{z0} + 2\tilde{B}_{\theta 0}\tilde{B}'_{z0}\tilde{J}'_{z0}/\tilde{B}^2_{z0} + 2\tilde{J}_{z0}\tilde{B}'_{z0}\tilde{B}'_{\theta 0}/\tilde{B}^2_{z0} \quad , \tag{21}$$

where the prime (') indicates derivatives with respect to x.

Having rewritten the Culham Model, a series of cases were run with pairs of increasing numbers (N,M) and for each pair, we looked at the variation of the growth rates with q_a and the character of the modes (by fixing q_a and varying S). In all cases considered up tp $(N,M)=(20,40)$, although the current profiles were reasonably flat and the growth rates increased considerably from the values they had with the standard Culham model where $(N,M)=(2,4)$, the character of the modes themselves were still tearing dominated modes. In search for the ideal modes we stretched these numbers to the limit of the computing machine and by running each case with different mesh size and time step as well as using double precision, we could establish the *optimum pair of numbers* $(N,M) = (32, 60)$ with which the numerical output were still reliable. In what follows we present the results for cases which employ this pair.

Fig.5 shows a plot of growth rates P and the singular surface position x_s against q_a for cases employing the following relevant entry data: $(N,M)=(32,60)$, $m=2$, $k_z=-0.25$ $(n=1)$, $S=1000$, $\tilde{R}_w=1.4$, $\tilde{R}_0=4.$, $J_{MAX}=501$, $N_{MAX}=800$. The unstable modes were found in the interval $1.36 \leq q_a \leq 2.24$ and the maximum growth rate occurred at $q_a=1.85$ with the value 70.88. The same comments as before apply to the x_s-curve. Figs. 6(a), (b) show the equilibria and perturbed profiles for the fastest growing mode $(q_a=1.85)$, where one can see how flat the equilibria current profile has become as compared to the ones used in the standard Culham model (see fig.4(a)); the perturbed profiles can also be seen packed around the singular surface with V_{r1} crossing the axis and, at first sight, this mode seems to be a tearing-like mode. To be sure of

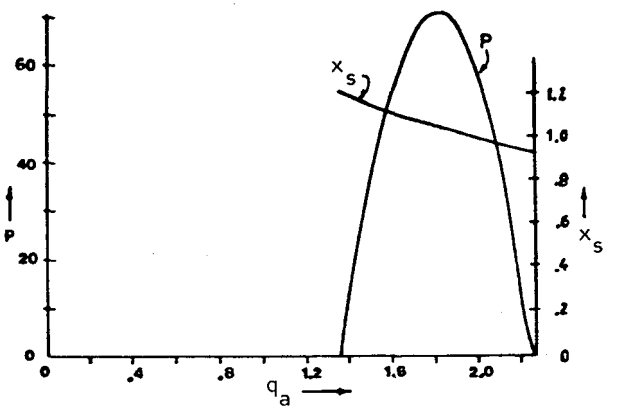

Fig.5 - The growth rate P and the singular surface radius x_s as a function of q_a for the Culham Model with $(N,M)=(32,60)$.

its nature however, a series of cases were run with q_a fixed at thevalue 1.85 and various values of S; the corresponding growth rate against S is presented in fig.7. Figs.8(a), (b) show just two of these cases to illustrate the behaviour of the B_{r1} and V_{r1} profiles (as we have done before), where one can see that from S=2000 to S=5000, B_{r1} remainsalmost unaltered whereas the point where V_{r1} crosses the axis shifts towards the singular surface; the fastest growing mode is therefore a tearing dominated mode. The rate at which the growth rates increased with S as compared with the standard Culham Model (see fig.1) is significant, as shown by the slope of the curve in fig.7, from $S\sim 2\times10^3$ up to 10^4. The slope is now given by K=0.826 and comparing this case with the standard Culharn Model (K=0.76) at S=5000 one concludes that the growth of the resistive modes is now 1.75 times faster than the standard case, These modes however are still tearing dominated ones. This is perhaps due to the rather low value of S we are usíng. In order to reach the Sscaling, values up to 10^5 should be used, which is not possible with the present working code.

Having failed to find near-ideal modes with the previous model, one might think that the absence of a vacuum region in that model could account for the absence of ideal ($kink$) modes. At this point we recall

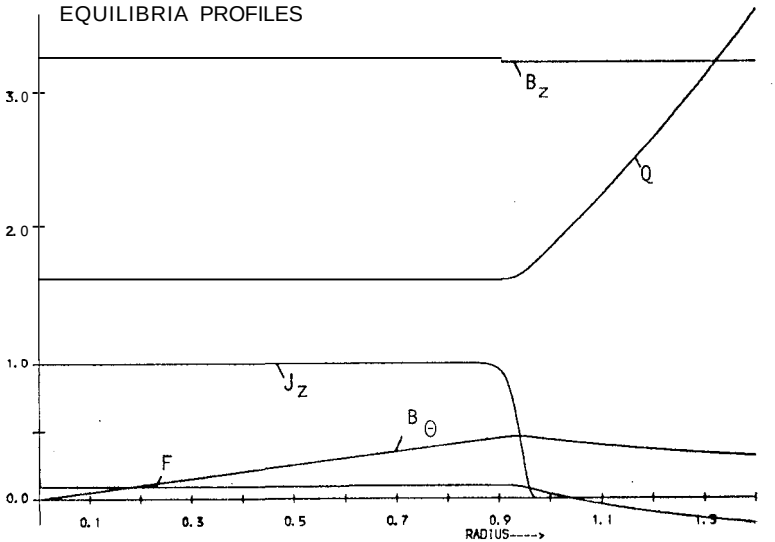

6(a)

B_{zo}=3.30277, B_{za}=3.23598 , B_{ta}=0.43729 , R_s=1.03975 , F_o=0.08986, Q_o=1.65139

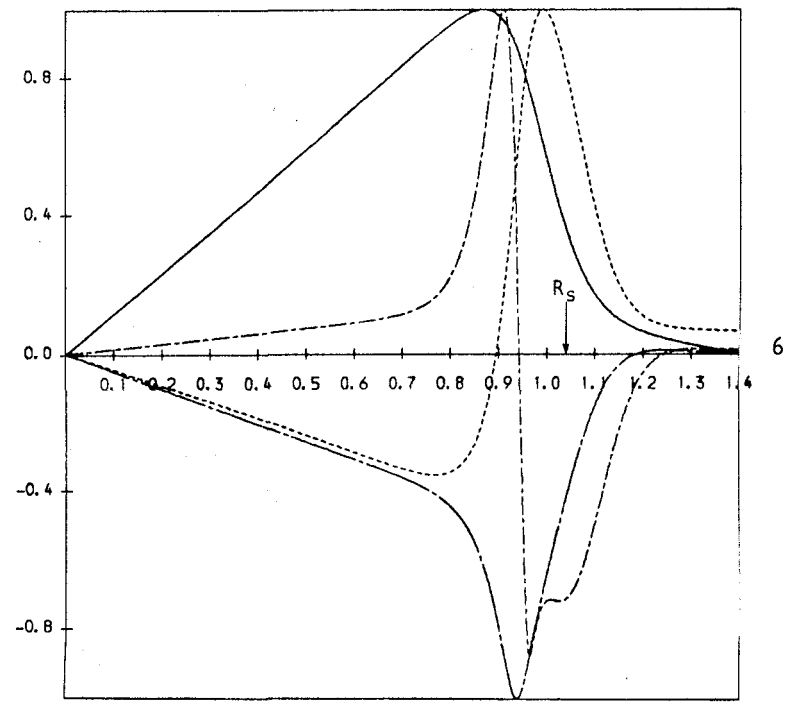

6(b)

Figs.6(a),(b) - (a) Equilibria and (b) perturbation profiles with q_a = 1.85, (N,M) = (32,60).

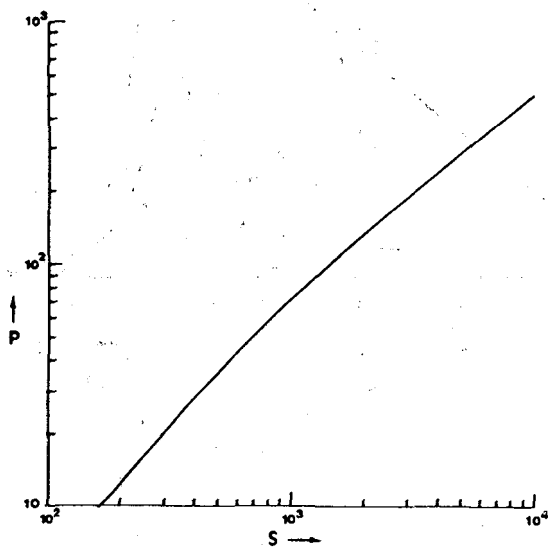

Fig.7 - Growth rate P versus S for the flat current profile with q =1.85, (N,M)=(32,60).

that for all the cases we have considered, the resistivity was set equal to a constant (η=1.) throughout the plasma (in contact with the conducting wall). In order to simulate a vacuum, we have raised the resistivity outside the current channel by using the formula

$$\tilde{\eta}(x) = 1/(\tilde{J}_{z0}(x) + \delta_r) \ , \qquad (22)$$

and run similar cases again.

Fig.9 shows the growth rate P and the singular surface radius x_s plotted against q_a for a number of cases with δ_r = 0.05, meaningthat outside the current channel where $\tilde{J}_z$=O we have now a twenty times more resistive plasma than inside the current channel, i.e., S_{edge}=50. The relavant entry data for running these cases were as follows: m=2, k_z = =-0.25, S=1000, $\tilde{R}_w$=1.5, $\tilde{R}_0$=4.0, (N,M)=(32,60), J_{MAX}=501, N_{MAX}=2000.

The maximum growth was found at q_a=1.80 with the value 123.17, and the interval where the unstable modes were found was $1.31 \leq q_a \leq 2.25$. Although we have a different $\tilde{R}_w$ from the previous cases with constant resistivity (η=1, and $\tilde{R}_w$=1.4), we can see here an almost twofold in-

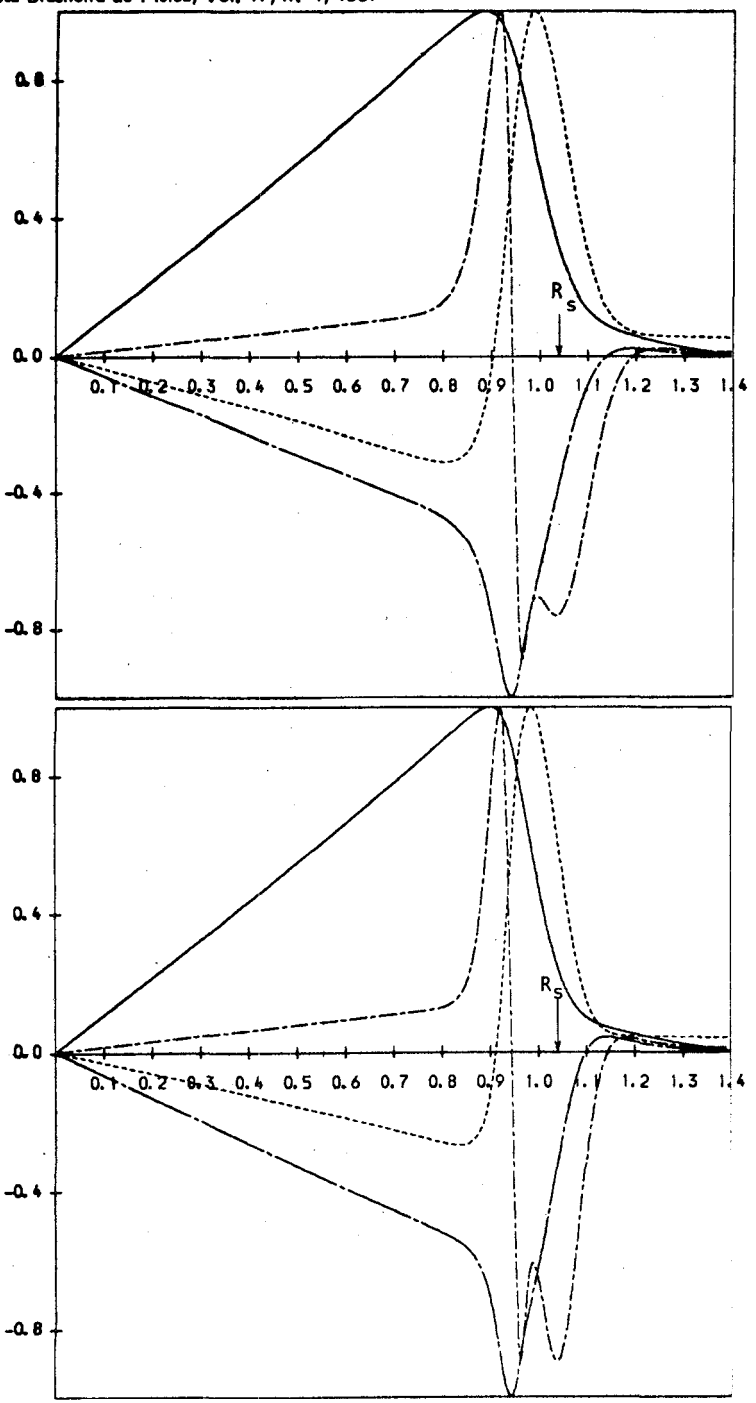

8(a)

8(b)

Figs.8(a),(b) - Perturbed profiles with S=2000 and (b) S=5000, both with q_a=1.85.

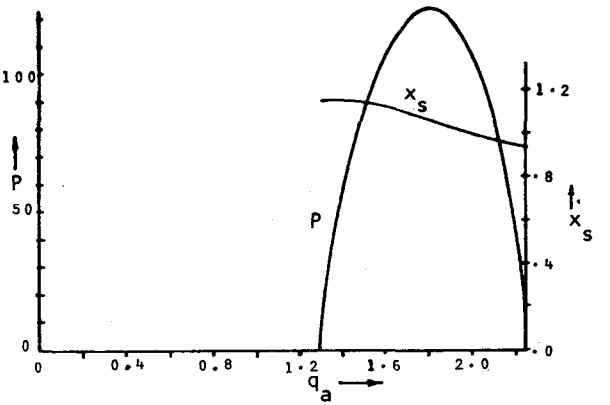

Fig.9 - Plots P versus q_a and x_s versus q_a for the Culham Model with $(N,M)=(32,60)$ and resistivity profile ($\delta_r=0.05$, $\tilde{\eta}=20.$ for $x>1$).

crease on the maximum growth rate (compare fig.9 with fig.5); the interval of q_a for unstable modes however did not change appreciably. Again, in order to look at the nature of the growing modes, we have run cases where q_a was fixed at 1.80 (the fastest at S=1000) and q_a=2.0 and S was varied; the results are represented in fig.10. The curve with q_a=2.0 has a slightly greater slope (K=0.95) than the one with q_a=1.8 (K=0.89) in the interval shown ($S \sim 10^2$-10^4) which indicates that the maximum in fig. 9 may shift slightly to the right (along the q_a axis) for $S > 10^4$. The values of K for both curves suggest however that with the insertion of a vacuum, between the current channel and the wall simulated with a higher resistivity in this case, the resistive modes will grow faster than in previous models, approaching the ideal MHD case of K=1. In all these cases however, the tearing mode character still seems to dominate, as one can infer by applying the same analysis as before in figs.11(b), (c) for the cases with q_a=1.80 and S=1000 and S=10000. However, now S_{edge}=50 and the magnitude of P and scaling with S seem to indicate that this would be an ideal mode which would become apparent with higher S ($\sim 10^8$).

(b) Numerical results for the step model

In so far as the nature of the modes is concerned we have not

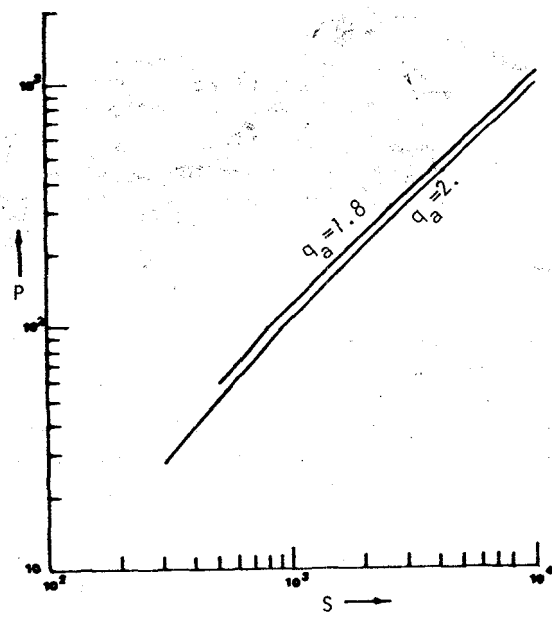

Fig. 10 - Same as for fig. 9 except plot P versus S.

been able to pinpoint a clear case of a kink dominated mode with the previous models. Is the flatness of the current profile not enough to generate such modes? Is the *vacuum* resistivity not high enough to simulateit?

To answer these questions we beqin by first considering thecase of a constant resistivity profile ($\eta(x)=1.$, $0 \leq x \leq \tilde{R}_w$) in the extrerne limit of current flatness, viz., the step model for it was not possible with the Culham model to raise the numbers M and N much further without getting meaningless numerical results from the code. In order to avoid infinities in the gradients of J_{z0}, $B_{\theta 0}$ and B_{z0} however, we defined these quantities in a separate routine within the code as follows:

$$J_{z0}(x) = \begin{cases} 1. & , x < 1 \\ 0 & , x > 1 \end{cases} \tag{23}$$

$$B_{\theta 0}(x) = \begin{cases} x/2 & , x \leq 1. \\ 1/2x, & x \geq 1. \end{cases} \tag{24}$$

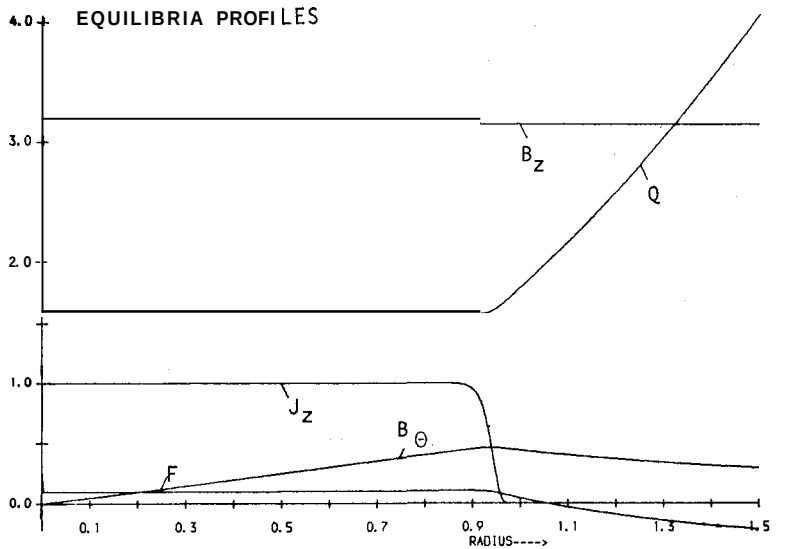

11 (a)

B_{zo}=3.21600, B_{za}=3.14889, B_{ta}= 0.43756, R_s=1.05435, F_o=0.10244, Q_o=1.60800

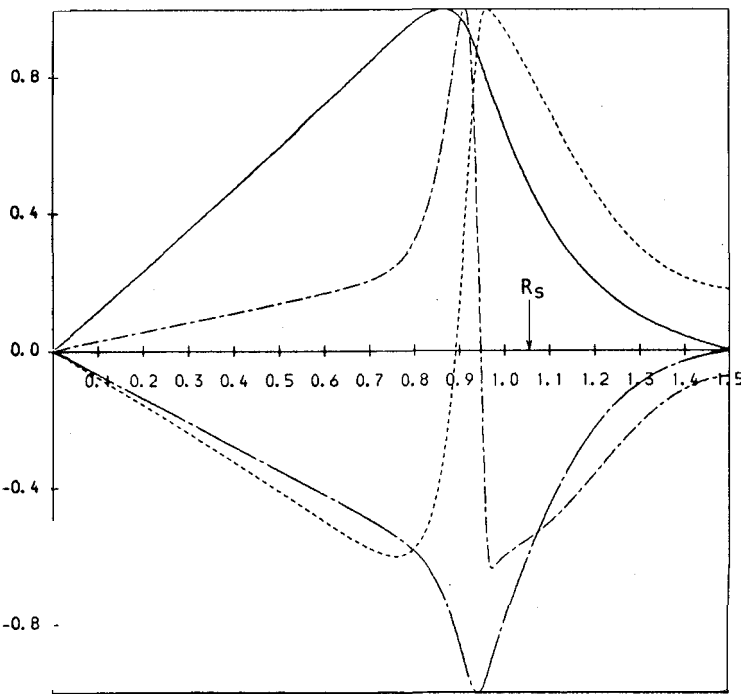

11 (b)

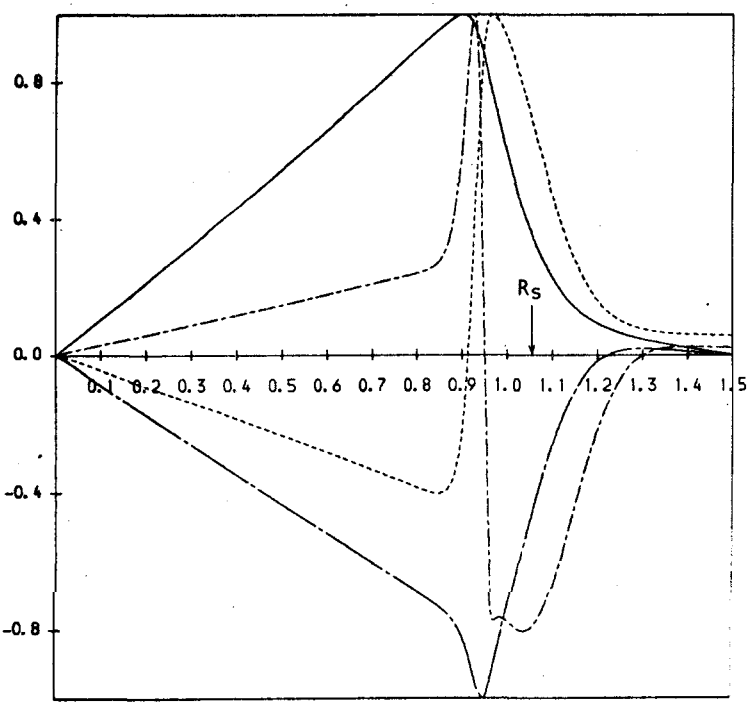

11(c)

Figs. 11(a),(b),(c) - Profiles for the Culham Model with (N,M)=(32,60), $\tilde{\eta}$=20 for x > 1, of the equilibria (a) and the perturbation with (b) q_a=1.8 and S=1000 and (c) q_a= =1.8 and S=10000.

$$\tilde{B}_{z0}(x) = \begin{cases} \left[\tilde{B}^2_{z0}(1) + (1-x^2)/2\right]^{1/2} , & x \leq 1 \\ \tilde{B}_{z0}(1) = q_a \tilde{R}_0/2 , & x \geq 1 \end{cases} \tag{25}$$

$$\tilde{J}'_{z0}(x) = \tilde{J}''_{z0}(x) = 0 \qquad \text{everywhere,} \tag{26}$$

$$\tilde{B}'_{\Theta 0}(x) = \begin{cases} 1/2 , & x \leq 1 \\ -1/2x^2 , & x > 1 \end{cases} \tag{27}$$

$$\tilde{B}''_{\Theta 0}(x) = \begin{cases} 0 , & x \leq 1 \\ 1/x^3 , & x > 1 \end{cases} \tag{28}$$

$$\tilde{B}''_{\Theta 0}(x) = \begin{cases} 0 , & x \leq 1 \\ -3/x^4 , & x > 1 \end{cases} \tag{29}$$

$$\tilde{B}'_{z0}(x) = \begin{cases} -x/2\tilde{B}_{z0}(x) , & x \leq 1 \\ 0 , & x > 1 \end{cases} \tag{30}$$

$$B''_{z0}(x) = \begin{cases} -(1+2\tilde{B}'^{2}_{z0}(x))/2\tilde{B}_{z0}(x) , & x \leq 1 \\ 0 , & x > 1 \end{cases} \tag{31}$$

$$\tilde{B}'''_{z0}(x) = \begin{cases} \dfrac{\tilde{B}'_{z0}(x)}{\tilde{B}^2_{z0}(x)}\,(1 + 2\tilde{B}'^{2}_{z0}(x)) - \dfrac{\tilde{B}'_{z0}\,\tilde{B}''_{z0}}{\tilde{B}_{z0}} , & x \leq 1 \\ 0 , & x > 1 \end{cases} \tag{32}$$

The finite discontinuities in the equations above present no numerical problems for the running of the code, for before considering cases of interest we have made various tests by varying the mesh size and time step and the results from each test did not very significantly.

In fig.12 we present plots of the growth rate versus q_a for a series of cases with different $\tilde{R}_w$'s of the unstable modes yielded by this model. The relevant data set used were as listed: m=2, k_z=-0,25, S=1000, $\tilde{R}_W$=4.0, J_{MAX}=501, N_{MAX}=2000, for each $\tilde{R}_W$=1.2,1.3,1.4,1.5,1.6,1.7.

The singular surface radius x_s can be shown to obey the relation $x_s=(2/q_a)^{1/2}$ for the step model, i.e., independent of $\tilde{R}_w$, and its plot against q_a is also inserted in the figure, illustrating the limit of validity of the curves for the description of the range in q_a where the equations are solved correctly. This is because near and on the left of the vertical broken lines the boudary conditions are violated, i.e., the singular surfases (where $\vec{k}.\vec{B}$=0) fall near $r=\tilde{R}_w$ or outside it. Therefore, the segments of the curves on the left of the broken lines, for each $\tilde{R}_w$, can be discarded from our analysis (they are, perhaps, spurious edge modes).

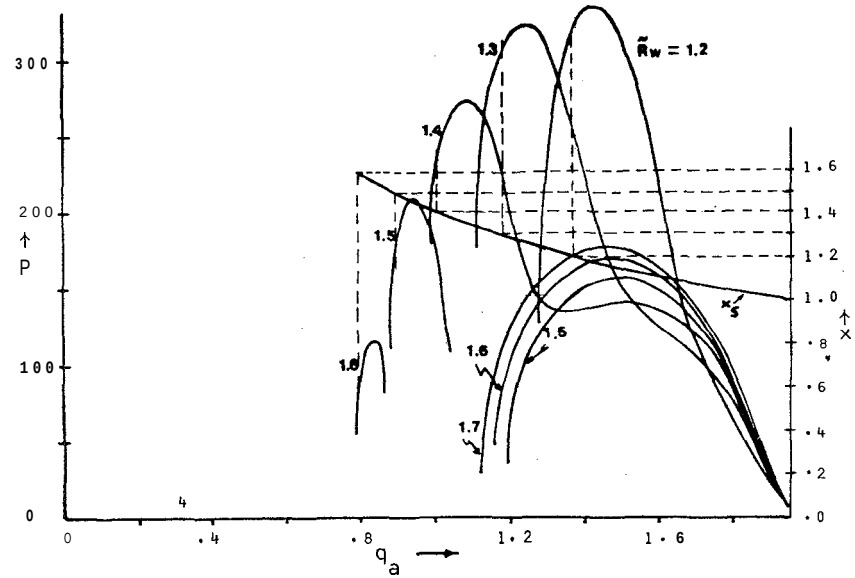

Fig. 12 - Growth rate P and the singular surface radius x_s as a function of q_a for the step model with $\tilde{\eta}$=1 throughout the plasma radius and $\tilde{R}_w$=1.2,1.3,1.4,1.5,1.6,1.7.

The following table 1 lists the main characteristics of these curves, with q_{amin} and q_{amax} denoting the minimum and the maximum q_a for instability, $P_{max}(q_a^*)$ standing for the maximum growth rate found at $q_a = q_a^*$ (two values in the case of two branches) and the last column listing the stability window in q_a between q_{amin} and q_{amax}.

In what follows, we present the characteristics of the unstable modes found on the curves in fig.12 for the cases $\tilde{R}_w$=1.2 and $\tilde{R}_w$=1.5, for all the other curves show modes with similar behaviour.

Fig.13 shows the equilibrium profiles for the 1st case presented in figs.14; these equilibrium profiles are very similar to all the other cases and for this reason we will omit them hereafter. In figs. 14(a),(b), we present the perturbed profiles for two cases with $\tilde{R}_w$ = 1.5 at S=1000, viz., q_a=1.5 and 1.9 and in figs. 15(a), (b), we present similar runs for S=5000. A close look at figs. 14 and 15 shows a kink-like behaviour according to the criterion employed before. Such a criterion however fails for cases picked up close to and on the left of

Table I - Characteristic values from the plots of the growth rate versus the step model parameter.

$\tilde{R}_w$	q_{amin}	q_{amax}	$P_{max}(q_a^*)$	stability window
1.2	1.275	1.95	331.98(1.40)	
1.3	1.11	1.95	317.22(1.20)	
1.4	0.98	1.95	274.48(1.10)	
1.5	0.88	1.95	208.92(0.95), 157.72(1.50)	(1.04, 1.19)
1.6	0.79	1.95	114.93(0.85), 170.15(1.50)	(0.87, 1.15)
1.7	1.115	1.95	177.01(1.50)	

EQUILIBRIA PROFILES

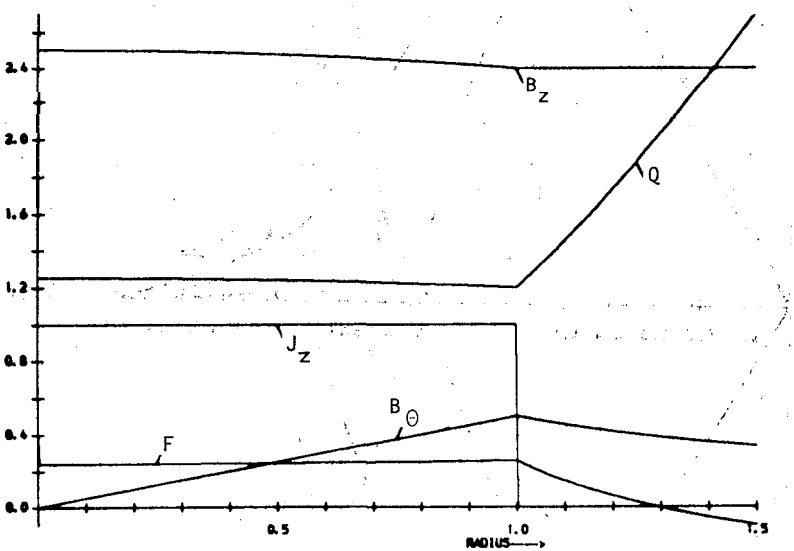

B_{zo}=2.50200, B_{za}=2.40021, B_{ta}=0.49950, R_s=1.29100, F_o=0.23865, Q_o=1.25100

Fig.13 - Equilibria profiles for the step model with q_a=1.2, $\tilde{R}_w$=1.5, S=1000.

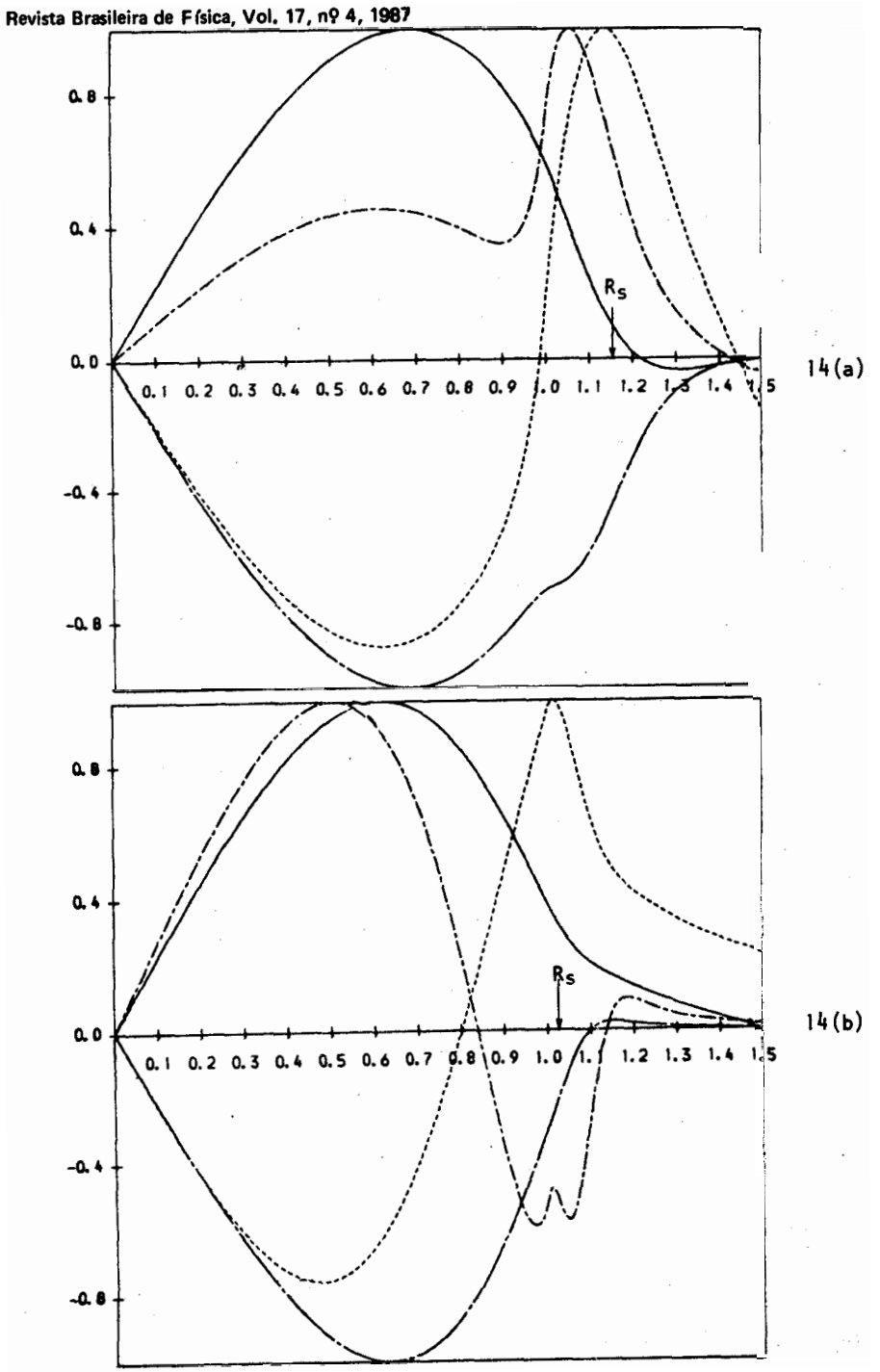

Figs.14(a),(b) - The perturbed profiles for the step model with (a) q_a=1.5 and (b) q_a=1.9 and a common R_w=1.5 at S=1000.

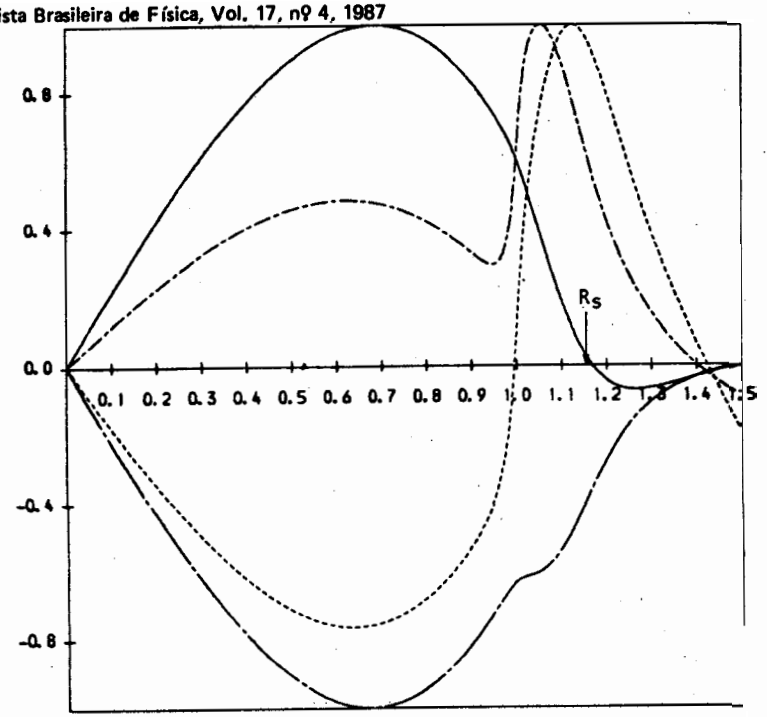

15(a)

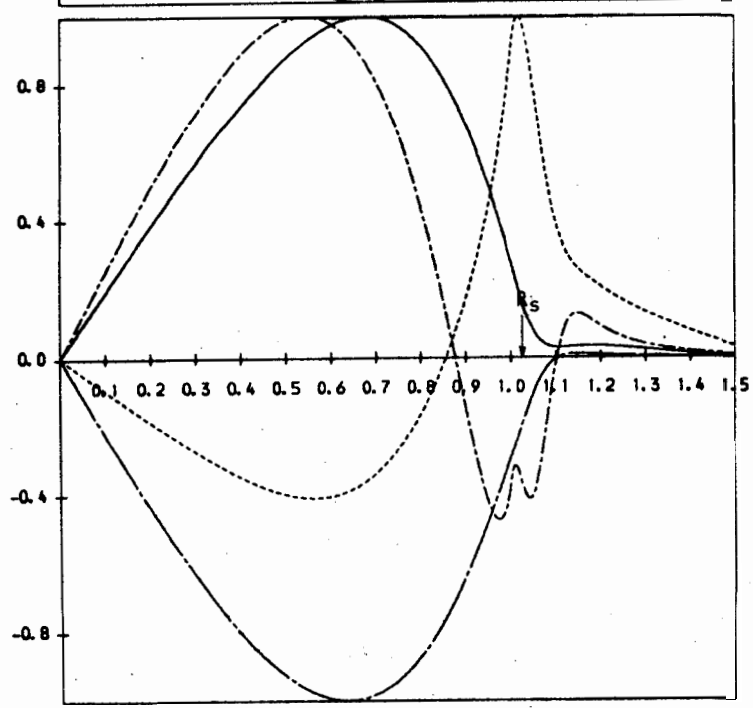

15(b)

Figs.15(a),(b) - Same as for fig. 14 except S=5000.

the point where the vertical broken lines in fig.12 intersect the curves (where the boundary conditions are invalid). We can say however that, apart from the regions in q_a situated on the far left of the broader branches of the curves in fig.12, most of the cases represented there are kink dominated modes.

Fig.16 shows the variation of the growth raté P versus S for cases with two distinct radii and three distinct q_a's. With $\tilde{R}_w=1.2$, the linear region is reached at S - 500 and persists up to S ~ 3×10^3 with the slope given by K = 1.12, after which the slope grows but the curve does not seem to reach another linear region. For the case with $\tilde{R}_w=1.5$ the linear region is around S ~ 3×10^3 with slopes K = 1.05 and K = = 1.42 for q_a = 1.5 and q_a = 1.9 respectively, and the slope grows beyond the value K = 1.37 in the former case but for S - 10^4 decreases to K = 1.33 for the latter. Although these last figures should riot be taken too seríously due to the limitation of the code for high values of S, the overall results indicate nevertheless that it is possible to have an unstable mode (ideal dominated in these cases) growing faster than the ones found in the ideal MHD limit (K=1).

Having found the unstable ideal modes with the step model with constant resistivity throughout the plasma ($\tilde{\eta}(x)=1, 0 \leq x \leq \tilde{R}_w$) the next task was trying to improve the model in order to get higher growth rates for kinks by simulating a vacuum between the current channel and the wall, i.e., by raising the resistivity in that region as we done before (see chapter 4 (a)). One can see, from formula (22), that the resistivity has now a step-like form, viz., $\tilde{\eta}=1$, $x \leq 1$; $\tilde{\eta}=1/\delta_r$, $x>1$.

In fig.17 we show plots of growth rates versus q_a for two distinct values of the (normalized) resistivity outside the current channel, viz., $\tilde{\eta}$=20. and $\tilde{\eta}$=50. with a fixed $\tilde{R}_w$=1.5. The curve for $\tilde{\eta}$=1. (already described in fig.12) is also shown for comparison, as well as the curve in broken lines describing Shafranov's free-boundary step model[**]. One can see from this figure that with the inclusion of a *vacuum* region, the maximum growth raises by almost four times -more precisely, P_{max}=419.40 at q_a = 1.1 and 437.60 at q_a = 1.2 for $\tilde{\eta}$ = 20.0 and $\tilde{\eta}$ = 50.0 respectively - from the value it had with constant resistivity ($\tilde{\eta}$=1.O); at the same time, the range in q_a for instability almost doubles - more pre-

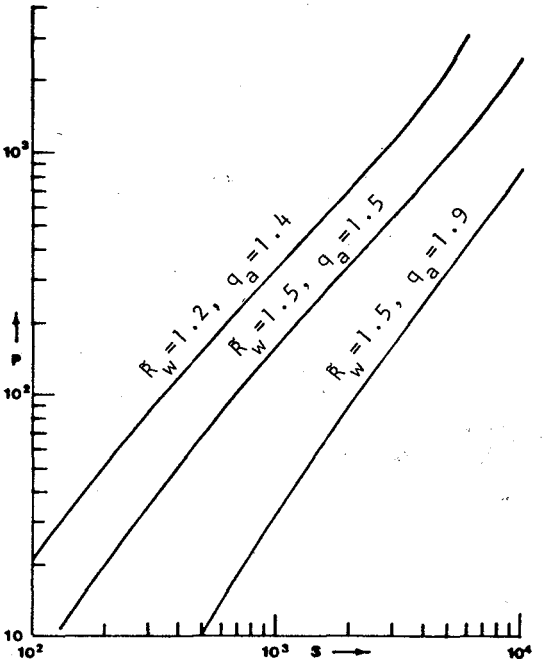

Fig.16 - Growth rate P versus S for the step model with constant resistivity with $\tilde{R}_w$=1.2, q_a=1.40 and $\tilde{R}_w$=1.5, q_a=1.5 and q_a=1.9.

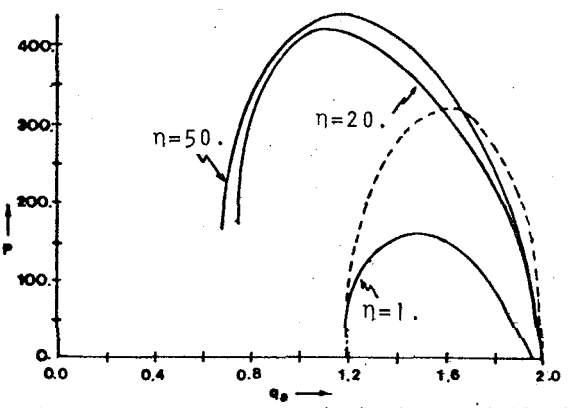

Fig.17 - Growth rate P versus q_a for the step model with resistivity profile ($\tilde{\eta}(x)$=20.,50. for $x>1$) and for the Shafranov's ideal step model broken lines ptotted from formula (32) of ref.6).

cisely, $0.743 \leq q_a \leq 1.99$ and $0.68 \leq q_a \leq 1.99$ for $\tilde{\eta} = 20.0$ and 50.0 respectively. For $\tilde{\eta} > 50.0$, strong numerical instabilities are set up in the code and the output results are rendered meaningless. The relevant input parameters for these cases were as listed: $m=2$, $k_z=-0.25$, $S=1000$, $\tilde{R}_W=1.5$, $\tilde{R}_0=4.0$, $N_{MAX}=2000$, $J_{MAX}=501$, for both $\tilde{\eta}=20.0$ and $\tilde{\eta}=50,0$ respectively.

We note that the curves exhibited in fig.17 for $\tilde{\eta}=1$ and the ideal case (broken lines) have nearly the same interval for instability. Also, as already pointed out, a constant resistivity extending outside the current channel introduced a further interval for instability as shown in the left branch of the curve $\tilde{R}_w=1.5$ in fig. 12; the step rises in resistivity (curves $\tilde{\eta}=20.0$ and $\tilde{\eta}=50.0$) outside the current channel have now enlarged and connected-these separate regions.

Figs.18(a), (b) illustrate the typical profiles of the perturbed quantities of the modes found for the case $\tilde{\eta}=50.0$ with $q_a=1.2$ and $S=1000$ and 5000 respectively, representing the fastest mode of the curve $\tilde{\eta}=50.0$ in fig.17. Its kink mode features are illustrated in figs. 18(a),(b), where B_{r1} crosses the axis with V_{r1} maintaining its sign. Cases with $\tilde{\eta}=20.0$ present identical features. Finally, in figs. 19 and 20 we present the variation of the growth rates with S for $\tilde{\eta}=20.0$ and 50.0 with $q_a=1.1,1.8$ and $q_a=1.2,1.9$ respectively. For fig. 19, the kink mode feature is more apparent (with B_{r1} crossing the axis) in the case $q_a=1.8$ than in the case $q_a=1.1$ (the fastest mode) where this feature shows up from $S\sim700$ upwards. The linear regions for both however are around $S\sim1000$ with approximately the same slope of $K=1.05$, i.e., near the ideal MHD limit of $K=1$. Fig. 20 presents similar cases for $\tilde{\eta}=50.0$ where the linear regions are around $S\sim10^3$ with slopes given by $K=1.06$ and $K=1.03$ for $q_a=1.2$ and 1.9 respectively. The slopes in both figures for higher values of S ($\sim10^4$) seem to indicate that the kink dominated modes found are much faster than in the linear region ($S\sim10^3$), which in its turn is a bit faster than the ones found in the ideal MHD limit ($K=1$).

5. CONCLUSION

We can now draw some conclusions of the work done as described

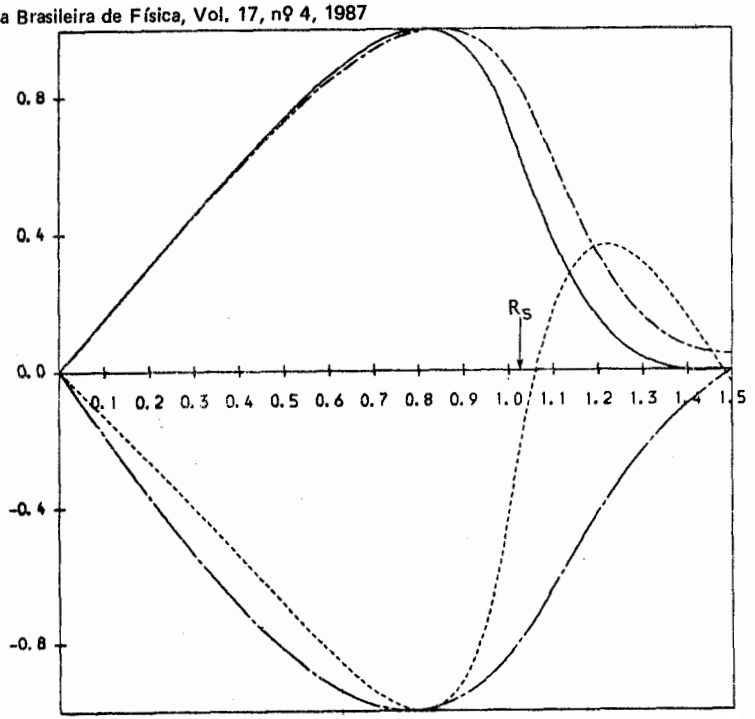

18(a)

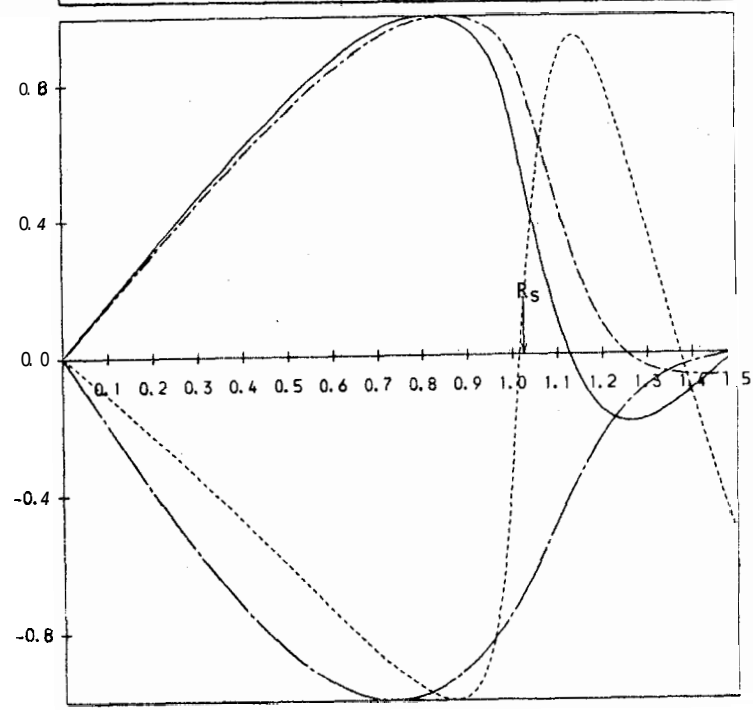

18(b)

Figs.18(a),(b) - Perturbed profiles for the step model with resistivity profile ($\tilde{\eta}$=50.) with q_a=1.9 and (a) S=10 and (b) S=5×10^3.

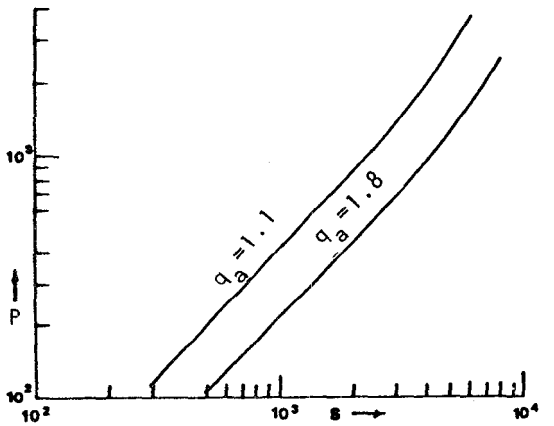

Fig.19 - Growth rate P versus S for the step model with a resistivity profile ($\tilde{\eta}$=20.) with q_a=1.1 and q_a=1.8.

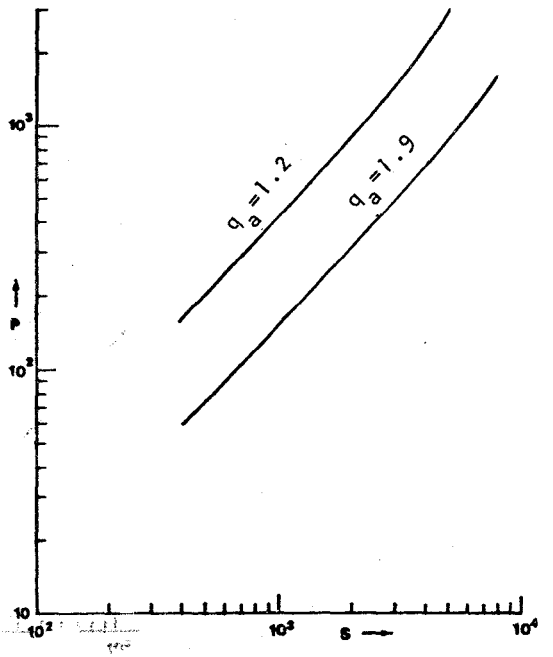

Fig.20 - Same as for fig.19, except q_a=1.2, 1.9 and $\tilde{\eta}$=50.

in previous chapters with the aid of the following table 2.

Table 2 - Main characteristics of the nodels used in this work

model studied	$\tilde{R}_w$	mode nurnbers m/n	interval of q_a for instability	$P_{max}(q_a)$ at S=1000 at S=10⁶	value of $\tilde{\eta}(x>1.)$	slope K	character of modes
Culham Model, N=2, M=4	1.4	2/1	(1.77,3.60)	28.97(2.4)	1.	0.76	tearing
		3/2	(1.514,2.70)	7.36(1.8)	1.	0.756	
Culham Model, N=32 M=60	1.5	2/1	(1.36,2.24)	70.88(1.85)	1.	0.826	tearing
Culham Model, resist. profile	1.5	2/1	(1.31,2.25)	123.17(1.80)	20.	0.89	tearing
step model	1.2	2/1	(1.275,1.95)	331.98(1.40	1.	1.12	kink
	1.5	2/1	(0.88,1.04 and (1.19,1.95)	208.92 (0.95) and 157.72(1.50)	1.	1.05	
step model resist. profile	1.5	2/1	(0.743,1.99)	419.40(1.1)	20.	1.05	kink
			(0.68,1.99)	437.60(1.2)	50.	1.06	
Shafranov's step model	1.5	2/1	(1.197,2.0)	316.82(1.59)	∞	1.0	kink

Inspection of the above table indicates that the maximum growth rate increases with the flatness of the current profile, as one would expect from known analytical results. The insertion of a *vacuum* region between the current channel and the wall has also contributed to the increase of the rnaximurn growth rate; the onset of kinks however did not seern to depend on the existence of a vacuum region, as can be seen in

the fourth line of the table (the step model with $\tilde{\eta} = 1.0$) although these kinks have their maximum growth increased when the *vacuum* was inserted back (fifth line). One can also see that from the standard Culham Model (N=2, M=4) to the flat one (N=32, M=60) with resistivity, the maximum growth has increased about four times; from the same oneto the step model with resistivity profile (fifth line), the increase is about 15 times at S=1000, The rates at which the growth rates increase with S have also gone up towards the K=I ideal MHD limit (last line) revealing the appearance of kink dominated modes in the latter models studied.

One may conjecture therefore that tearing modes found with the standard Culham Model would be suitable for describing the beginning of the process of disruption, whereas the tearing modes found with the Culham Model with N=32, M=60 would be suitable for the final stage of the disruption if the process is not so fast (~1sec); alternatively, the kink modes found in the step model with resistivity profile (or a Culham Model with N >> 32, M >> 60) might be the ones which are associated with the fast growing mode preceding disruption.

The results obtained in this work are, of course, limited in many aspects. One of them is that we are dealing with a linear, one dimensional code and therefore saturation of the modes cannot be predicted. The other one is that the code only gives realiable numerical results for the m=2 modes for $S \leq 10^4$. The destabilization of other modes by the m=2, n=I mode can only be accessed with a mode-coupling/quasi--linear code, so one cannot be sure about the role of the m=3, n=2 mode in the final stage of the disruption, The results nevertheless give an indication of the order of magnitude of growth rates and variation with S which may be relevant to major disruptions and leave open the question whether the final cause might be a tearing or a kink mode, or whether a tearing mode would after all evolve to a kink mode.

The author thanks Culham Laboratory, UK, for the use of its facilities and Dr, D.C.Robinson for his suggestion of this work and helpful discussions, as well as Mr.Paul Haynes for his invaluable advice on the existing computing system at Culham. The author is also

indebted to Dr.A.Montes, from INPE, Brasil, for his help on a numerical scheme used in this work.

The author was partially supported by Conselho Nacional de Desenvolvimento Científico e Tecnológico (CNPq), Brasil.

REFERENCES

1. M.F.Turner, J.A.Wesson, Nuclear Fusion 22, 8, 1069 (1982).
2. R.B.White, D.A.Monticello, M.N.Rosenbluth, Phys.Rev.Lett. 39, 25 1618 (1977).
3. B.V.Waddell, B.Carreras, H.R.Hicks, J.A.Holmes, D.K.Lee, Phys. Rev. Lett. 41, 20, 1386 (1978).
4. D.C.Robinson, private communication.
5. D.C.Robinson, Workshop on Physical Processes in Toroidal Confinement, Varenna, August 1985, with the paper "Resistive Process in Toroidal Confinement".
6. A.Tomimura, Rev.Bras.Fís., Vol.*17*, n? 3, 401 (1987).
7. J.Killeen, in *Physics of Hot* Plasmas, Ed.Plenum Press, N.Y., 1970.
8. J.A.Dibiase, J.Killeen, Journal of Computational Physics 24, 158 (1977).
9. D.C.Robinson et *al.*, Culham Laboratory Report CLM-P710, Sept.1983.
10. H.P.Furth *et al.*, The Physics of Fluids, 6, 4, 459 (1963).
11. J.E.Crow et *al.*, Proc. 6th European Conference on Controlled Fusion and Plasma Physics, Moscow, 1973.
12. A.H.Glasser *et* al., Physics of Fluids 18, 875 (1975) and 19, 596 (1976).
13. H.P.Furth *et* al., Physics of Fluids *16*, 1054 (1973).
14. V.D.Shafranov, Soviet Physics-Technical Physics, *15*, 2, 175 (1970).

Resumo

Trabalho numérico foi realizado com um código MHD resistivo, linear e unidimensional oqual resolveum sistema deequações para a instabilidade HHD resistiva nos vários parâmetros relevantes da perturbação. Um número de modelos com as configurações do equilíbrio consistentes com aquelas encontradas nos processos disruptivos em tokamaks foram considerados e alguns dos modos instáveis obtidos com o código foanalisados do ponto de vista de suas reais naturezas (se do tipo "tear-

ing" ou do tipo "kink"), de suas razões de crescimento e do numero magnético de Reynolds S (com respeito ao campo magnético poloidal na posição do raio do canal de corrente). Em particular, as condições para o crescimento do modo $m = 2$, $n = 1$ num certo número de configurações de equilíbrio foram estudadas levando em conta o grau de achatamento do perfil da densidade de corrente, assim como o valor relativo da resistívidade entre o canal de corrente e a parede condutora. O caráter do modo do tipo "tearing" nos modos instáveis estudados prevaleceu em quase todos os casos considerados apesar dos grandesvaloresde S e do alto grau de achatamento nos perfis das densidades de corrente usados em algumas dessas configurações. Os modos ideais do tipo "kink" só puderam ser encontrados no caso extremo do modelo escada.